Applied Mathematics and Computation 461 (2024) 128298

Contents lists available at ScienceDirect

Applied Mathematics and Computation

journal homepage: www.elsevier.com/locate/amc

Modeling and Passivity-Based Control for a convertible fixed-wing VTOL

J.E. Durán-Delfín [a], C.D. García-Beltrán [a,*], M.E. Guerrero-Sánchez [b], G. Valencia-Palomo [c], O. Hernández-González [c]

[a] Tecnológico Nacional de México, Centro Nacional de Investigación y Desarrollo Tecnológico, Interior Internado Palmira S/N, Col. Palmira, Cuernavaca, Morelos, Mexico
[b] IIxM CONAHCYT/Tecnológico Nacional de México, I.T. Hermosillo, Av. Tec. 115, 83170, Mexico
[c] Tecnológico Nacional de México, I.T. Hermosillo, Av. Tec. 115, 83170, Mexico

ARTICLE INFO

Keywords:
Convertible VTOL
Hybrid UAV
Passivity-Based Control
Control allocation

ABSTRACT

This article presents a mathematical model and a controller for a convertible fixed-wing Vertical Take-Off and Landing (VTOL). The mathematical model considers the aerodynamic forces generated by the motors. The developed Passivity-Based Control (PBC) law stabilizes the rotational and translational dynamics of a convertible Unmanned Aerial Vehicle (UAV) in the transition stages of cruise-stationary flight. The control objective is to allow the realization of the two flight regimes of a convertible VTOL along a trajectory. A control assignment technique is also presented that allows the decoupling of the angles of the front motors so that they can have different positions. Finally, numerical simulations are carried out to validate the performance of the presented algorithm. The results indicate that this controller can provide enough maneuverability to track different trajectories with good performance.

1. Introduction

Unmanned Aerial Vehicles (UAVs) have rapidly expanded in a wide variety of industries. The two main designs of UAVs are fixed-wing aircraft and rotary motors helicopters. On the one hand, fixed-wing UAVs can fly at higher speeds, 40 to 60 kilometers per hour, even while taking pictures in the process, covering 2.5 square kilometers per hour [1]. On the other hand, UAVs with rotary motors can perform flying stationary in hover and be more precise in reduced spaces; however, they have shorter battery life because they usually operate with four or more motors but have the ability to achieve takeoffs and landings without the need for large terrain to carry out such activities [2].

Integrating the advantages of these two types of vehicles, the convertible fixed-wing Vertical Take-Off and Landing (VTOL) effectively combines hover abilities with cruise flight and vertical takeoff and landing; see, for instance, Fig. 1.

The mathematical model of a UAV can be represented by making use of Lie-group formalism. For example: [3] shows the use of Lie-group theory for dynamic-model-aided navigation of multirotor unmanned aerial vehicles. [4] describes a control law for a quadcopter drone based on the virtual attractive-repulsive potentials theory, where the quadcopter mathematical model is formulated

* Corresponding author.
E-mail addresses: m20ce075@cenidet.tecnm.mx (J.E. Durán-Delfín), cgarcia@cenidet.edu.mx (C.D. García-Beltrán), maria.guerreros@hermosillo.tecnm.mx (M.E. Guerrero-Sánchez), gvalencia@hermosillo.tecnm.mx (G. Valencia-Palomo), omar.hernandezg@hermosillo.tecnm.mx (O. Hernández-González).

https://doi.org/10.1016/j.amc.2023.128298
Received 13 January 2023; Received in revised form 22 June 2023; Accepted 14 August 2023

Available online 3 September 2023

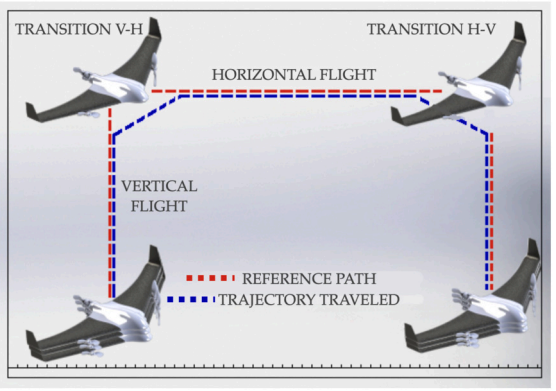

Fig. 1. Vertical and horizontal flight modes and transitions for a convertible fixed-wing VTOL.

on a Lie-group. Also, the mathematical model of the UAV can be based on classical 6-Degrees of Freedom (DOF) formalism which requires 12 main variables. In this paper, we present the Convertible Fixed-Wing VTOL mathematical model using the classical 6-DOF formalism.

The control design of a convertible VTOL is not trivial, considering that the flight dynamics of a fixed-wing UAV and a vehicle with rotary motors are quite different and often opposite. Thus, the control design problem for convertible UAVs is novel and has not been extensively investigated in the literature. For example, some works present linear control techniques such as a convertible Model-based Predictive Control (MPC) scheme that allows flight–mode conversion for a quad-tiltRotor UAV as developed in [5]. The mathematical model and a linear quadratic control algorithm to hover flying of a convertible UAV are introduced in [6]. In this case, the control scheme was developed for the longitudinal dynamic model of the vehicle. Other works do not consider the translational dynamics control of the UAV, e.g., [7], which developed a nonlinear mathematical model for the rotational dynamics of a convertible UAV. A robust finite time control algorithm and a robust integral of the signum of the error-based tracking control scheme were considered to stabilize the altitude and rotational dynamics, respectively. In [8], the mathematical model and a proportional derivative control strategy for a convertible UAV are shown. The numerical results demonstrate good flight control behavior; however, only the altitude and orientation dynamics were controlled. Moreover, in [9], the flight dynamics during a convertible tilt-wing VTOL transition stage is presented. A nonlinear mathematical model is developed, including the complete dynamics of the UAV, which presents significant changes in the aerodynamic characteristics, especially during the transition flight phase; however, only the altitude dynamic is controlled.

Other works present controllers for a simplified model of the convertible vehicle. In [10], the authors design transition optimization algorithms for a vertical takeoff and landing tail-sitter from a longitudinal aircraft model. A coupling between the angles of the frontal motors and a simplified mathematical model are considered. In [11], a control allocation algorithm for a convertible UAV is introduced. The control technique converts the high-level commands in terms of total desired thrust and torques into commands distributed among the vehicle's actuators. It is worth mentioning that fixed motors in the same angular position are considered, and the Y-axis is not considered in the mathematical model. The coupling between the angles of the frontal motors was also considered in [12], where an MPC algorithm for a convertible tilt-quadrotor fixed-wing vehicle was developed. It combines vertical takeoff and landing capabilities with high-speed forward flight. Experimental results show the good performance of the controller. In [13], a nonlinear dynamic inverse method for the rotation control of a convertible UAV with a tailsitter layout and a high-lift airfoil is presented. Meanwhile, in [14], a Fused-Proportional Integral Derivative (F-PID) control approach for a tilt-quadrotor VTOL is designed. The F-PID consists of two separate PID algorithms, where one handles the fixed-wing vehicle, and the other is designed for multirotors. The output of both control strategies is fused depending on the airspeed to obtain an orientation setpoint and a tilt angle of the rotors. Also, in [15], a nonlinear MPC approach was introduced for a convertible UAV and a control allocation that distributes the required control actions between propellers, tilt servos, and control surfaces.

The results of these works are excellent, however, such works present some of the following drawbacks with respect to the model or mechanical configuration of a convertible fixed-wing VTOL:

- The aerodynamic forces generated by the motors are neglected.
- The rear motors have only one degree of freedom.
- Some works consider a coupling between the angles of the frontal motors. This implies that the angular positions of the frontal motors cannot be different.
- Also, some works only develop the mathematical model in two dimensions.

With respect to the controller, we have the following restrictions:

- Some works only consider the design of control strategies to hover flying.
- The controller design is based on a linearized model.

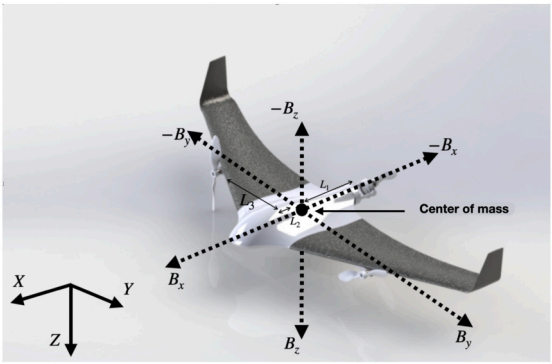

Fig. 2. Body-fixed coordinate frame $B = \{O_B, B_x, B_y, B_z\}$ and inertial coordinate frame $I = \{O_I, X, Y, Z\}$ for a convertible fixed-wing VTOL.

- Only constant reference tracking is tested.

Motivated by the aforementioned considerations, a novel mathematical model for a particular type of aircraft capable of performing vertical takeoffs and landings and cruise flights is designed in this work. The convertible vehicle considered in this work is a tilting-rotor fixed-wing VTOL UAV. This vehicle has a motor configuration similar to a tricopter, two front thrust motors, and one rear motor. It does not have a tail rudder or elevators. Moreover, the vehicle possesses four servomotors that tilt the position of both the front and rear motors, the angles of inclination of these motors are not coupled to each other, as in the traditional way, which allows them to be controlled independently. The tilt angle of the rear motor has two degrees of freedom that allows for generating thrust forces and moments in the three axes of the vehicle body, avoiding the need for elevators and a rudder. This novel mechanical configuration reduces the number of the vehicle's actuators and facilitates its control. The nonlinear mathematical model includes changes in aerodynamic characteristics during the transition flight.

In addition, a Passivity-Based Control (PBC) strategy that stabilizes the vehicle's rotational and translational dynamics in the transition stages of cruise-stationary flight is developed. Finally, an assignment algorithm is developed, which allows the decoupling of the angles of the front motors so that they can have different positions, obtain the tilt angles of the two degrees of freedom of the rear motors and obtain the rotational speeds of the three motors.

The paper is structured as follows: Section 2 presents the nonlinear model of a tilting-rotor fixed-wing VTOL UAV; Section 3 develops a nonlinear control strategy for the vehicle translational and rotational movements and a control allocation algorithm; Section 4 describes numerical simulations and their corresponding results; finally, Section 5 discusses the conclusions and perspectives.

2. Mathematical model

This section presents the mathematical model of a convertible fixed-wing VTOL. From Fig. 2, let us consider a body-fixed coordinate frame $B = \{O_B, B_x, B_y, B_z\}$ and an inertial coordinate frame $I = \{O_I, X, Y, Z\}$. The system is modeled considering six degrees of freedom $\lambda = \begin{bmatrix} \nu & \varrho \end{bmatrix}^T$, which includes three inertial position components $\nu = \begin{bmatrix} x & y & z \end{bmatrix}^T$ of the system center of mass relative to I, as well as the three Euler angles $\varrho = \begin{bmatrix} \theta & \phi & \psi \end{bmatrix}^T$ for the rotation of the vehicle; $\{u, v, w\}$ represents the linear velocity and $\{p, q, r\}$ the angular velocity defined with respect to B.

Some assumptions are proposed for achieving the main goal:

A1 The mass of the UAV remains constant.
A2 The vehicle is considered a rigid solid body.
A3 The earth is rotating about a fixed axis in the inertial space.
A4 The XZ plane of the VTOL body-fixed coordinate system is the symmetry plane.
A5 The centripetal acceleration associated with the earth's rotation is neglected.

The dynamic model is divided into two sets of dynamic equations, the first set of equations defines the translational motion of the system,

$$F_x - D - mg\sin\theta = m(\dot{u} + qw - rv);$$

$$F_y + N + mg\cos\theta\sin\phi = m(\dot{v} + ru - pw);$$

$$F_z - L + mg\cos\theta\cos\phi = m(\dot{w} + pv - qu);$$

in matrix form, it can be expressed as

Table 1
Table of parameters.

Parameters	Value	Units
m	3.1	kg
g	9.81	m/s^2
ρ	1.2041	kg/m^3
S	0.75	m^2
b, c	2.1, 0.3572	m
I_{xx}, I_{yy}, I_{zz}, I_{xz}	1.229, 0.1702, 0.8808, 0.9343	kg/m^2
L_1, L_2, L_3	0.57, 0.325, 0.129	m
K_F, K_M	1.97×10^{-6}, 2.88×10^{-7}	-
C_{D_0}, C_{D_α}, C_{D_q}	0.0101, 0.8461	-
C_{N_0}, C_{N_β}, C_{N_p}, C_{N_r}	3.205×10^{-18}, -0.195, -0.117, 0.096	-
C_{L_α}, C_{L_0}, C_{L_q}	4.0191, 0.0254, 3.8954	-
C_{l_0}, C_{l_β}, C_{l_p}, C_{l_r}	1.152×10^{-18}, -0.077, -0.402, 0.025	-
C_{m_0}, C_{m_α}, C_{m_q}	0.0180, -0.2524, -1.3047	-
C_{n_0}, C_{n_β}, C_{n_p}, C_{n_r}	-2.267×10^{-7}, 0.04, -0.025, -0.125	-

$$\begin{bmatrix} m & 0 & 0 \\ 0 & m & 0 \\ 0 & 0 & m \end{bmatrix}\begin{bmatrix} \dot{u} \\ \dot{v} \\ \dot{w} \end{bmatrix}+\begin{bmatrix} 0 & -mr & mq \\ mr & 0 & -mp \\ -mq & mp & 0 \end{bmatrix}\begin{bmatrix} u \\ v \\ w \end{bmatrix}-\begin{bmatrix} -mg\sin\theta \\ mg\cos\theta\sin\phi \\ mg\cos\theta\cos\phi \end{bmatrix}=C_m+F_m; \tag{1}$$

where m represents the UAV mass, the vector $F_m=\begin{bmatrix} F_x & F_y & F_z \end{bmatrix}^T$ contains the thrust forces in each axis of displacement with respect to B, the vector $C_m=\begin{bmatrix} -D & N & -L \end{bmatrix}^T$ represents the dissipative forces generated by the wind, which are the drag, side slide, and lift, respectively and these are calculated as follows:

$$D=\frac{1}{2}\rho SV^2C_D;\quad N=\frac{1}{2}\rho SV^2C_N;\quad L=\frac{1}{2}\rho SV^2C_L;$$

where ρ is the air density, S is the wing area, V denotes the airspeed in straight; C_D, C_N, and C_L are the aerodynamic coefficients. These parameters were calculated in wind tunnel tests performed on a commercial convertible UAV model Skywalker X8, which were obtained from [16,17]. These coefficients can be expressed in linear terms as [18]:

$$\begin{aligned} C_D(\alpha,q)&\approx C_{D_0}+C_{D_\alpha}\alpha+C_{D_q}\frac{c}{2V}q;\\ C_N(\beta,p,r)&\approx C_{N_0}+C_{N_\beta}\beta+C_{N_p}\frac{b}{2V}p+C_{N_r}\frac{b}{2V}r;\\ C_L(\alpha,q)&\approx C_{L_0}+C_{L_\alpha}\alpha+C_{L_q}\frac{c}{2V}q; \end{aligned}$$

where α is the angle of attack and β the side slip angle; C_{D_x}, C_{N_x} and C_{L_x} represents the drag, side, lift force coefficients, respectively. The values of the parameters and coefficients are shown in Table 1.

The second set of equations shows the rotational dynamics of the system:

$$\begin{aligned} L_A+M_x&=I_{xx}\dot{p}-I_{xz}(\dot{r}+pq)-\left(I_{yy}-I_{zz}\right)qr;\\ M_A+M_y&=I_{yy}\dot{q}-I_{xz}\left(r^2-p^2\right)-\left(I_{zz}-I_{xx}\right)pr;\\ N_A+M_z&=I_{zz}\dot{r}-I_{xz}(\dot{p}-qr)-\left(I_{xx}-I_{yy}\right)pq; \end{aligned}$$

they can be expressed in matrix form as follows:

$$\begin{bmatrix} I_{xx} & 0 & -I_{xz} \\ 0 & I_{yy} & 0 \\ -I_{xz} & 0 & I_{zz} \end{bmatrix}\begin{bmatrix} \dot{p} \\ \dot{q} \\ \dot{r} \end{bmatrix}+\begin{bmatrix} -I_{xz}q & -I_{yy}r & I_{zz}q \\ I_{xx}r+I_{xz}p & 0 & -I_{xz}r-I_{zz}p \\ -I_{xx}p & I_{yy}p & I_{xz}q \end{bmatrix}\begin{bmatrix} p \\ q \\ r \end{bmatrix}=\begin{bmatrix} L_A \\ M_A \\ N_A \end{bmatrix}+\begin{bmatrix} M_x \\ M_y \\ M_z \end{bmatrix}; \tag{2}$$

with

$$\begin{bmatrix} L_A \\ M_A \\ N_A \end{bmatrix}=\frac{1}{2}\rho SV^2\begin{bmatrix} C_{LA} \\ C_{MA} \\ C_{NA} \end{bmatrix};$$

where I_{xx}, I_{yy}, I_{zz} and I_{xz} are the inertia coefficients; M_x, M_y and M_z represent the torques generated by the motors with respect to B; C_{LA}, C_{MA}, and C_{NA} are the aerodynamic coefficients that produce angular momentum on each axis of the vehicle. These coefficients were also obtained through wind tunnel tests and are parameterized in linear terms as [18]:

$$\begin{aligned} C_{LA}(\beta,p,r)&\approx C_{l_0}+C_{l_\beta}\beta+C_{l_p}\frac{b}{2V}p+C_{l_r}\frac{b}{2V}r;\\ C_{MA}(\alpha,q)&\approx C_{m_0}+C_{m_\alpha}\alpha+C_{m_q}\frac{b}{2V}q; \end{aligned}$$

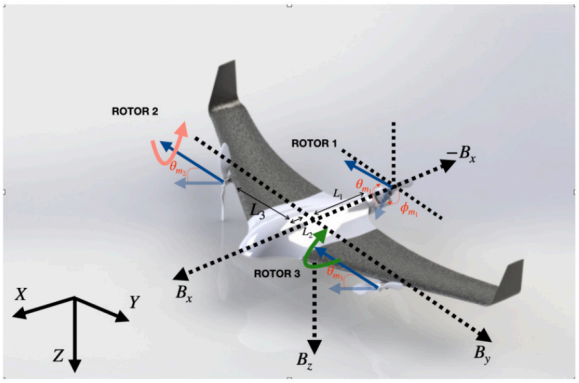

Fig. 3. Turning directions $\theta_{m_1}, \theta_{m_2}, \theta_{m_3}$ for motors 1-3 respectively of the convertible VTOL.

$$C_{NA}(\beta, p, r) \approx C_{n_0} + C_{n_\beta}\beta + C_{n_p}\frac{b}{2V}p + C_{n_r}\frac{b}{2V}r;$$

where C_{l_x}, C_{m_x}, and C_{n_x} represent the rolling, pitching, and yawing moments coefficients, respectively. The values of such coefficients are given in Table 1.

2.1. Euler–Lagrange formulation

From the Euler-Lagrange formulation, Eqs. (1) and (2) can be expressed as

$$\Delta\ddot{\lambda} + C(\dot{\lambda})\dot{\lambda} + G(\lambda) = C_m + F_m; \tag{3}$$

where Δ and $C(\dot{\lambda}) \in \mathbb{R}^{6\times6}$, $G(\lambda)$, C_m and $F_m \in \mathbb{R}^6$, these matrices and vectors are expressed as follows,

$$\Delta = \begin{bmatrix} m & 0 & 0 & 0 & 0 & 0 \\ 0 & m & 0 & 0 & 0 & 0 \\ 0 & 0 & m & 0 & 0 & 0 \\ 0 & 0 & 0 & I_x & 0 & -I_{xz} \\ 0 & 0 & 0 & 0 & I_y & 0 \\ 0 & 0 & 0 & -I_{xz} & 0 & I_z \end{bmatrix};$$

$$C(\dot{\lambda}) = \begin{bmatrix} 0 & -mr & mq & 0 & 0 & 0 \\ mr & 0 & -mp & 0 & 0 & 0 \\ -mq & mp & 0 & 0 & 0 & 0 \\ 0 & 0 & 0 & -I_{xz}q & -I_{yy}r & I_{zz}q \\ 0 & 0 & 0 & I_{xx}r + I_{xz}p & 0 & -I_{xz}r - I_{zz}p \\ 0 & 0 & 0 & -I_{xx}q & I_{yy}p & I_{xz}q \end{bmatrix};$$

$$G(\lambda) = \begin{bmatrix} -mg\sin\theta \\ mg\cos\theta\sin\phi \\ mg\cos\theta\cos\phi \\ 0 \\ 0 \\ 0 \end{bmatrix}; \quad C_m = \begin{bmatrix} -D \\ N \\ -L \\ L_A \\ M_A \\ N_A \end{bmatrix}; \quad F_m = \begin{bmatrix} F_x \\ F_y \\ F_z \\ M_x \\ M_y \\ M_z \end{bmatrix}.$$

2.2. Calculation of the forces and moments produced by the motors

Due to the ability of the motors to tilt, it is necessary to model the thrust forces generated by the motors with the help of trigonometric functions because when tilting in the direction of a particular axis, the forces are decomposed into more than one axis of motion.

In Fig. 3, we can see the directions of movement and the direction of rotation of the motors that were taken into consideration to perform the decomposition of forces.

Fig. 4 illustrates the components of aerodynamic force and the momentum generated by the motors in X, Y, and Z body directions.

The decomposition of the thrust forces in the X, Y, and Z axes of motion of the front motors 2 and 3 was obtained following the directions of motion in Fig. 4a and 4b, where the angles θ_{m_2} and θ_{m_3} are defined to represent the independent inclinations of both motors and to help us in the trigonometric decomposition of forces. These equations are represented as follows:

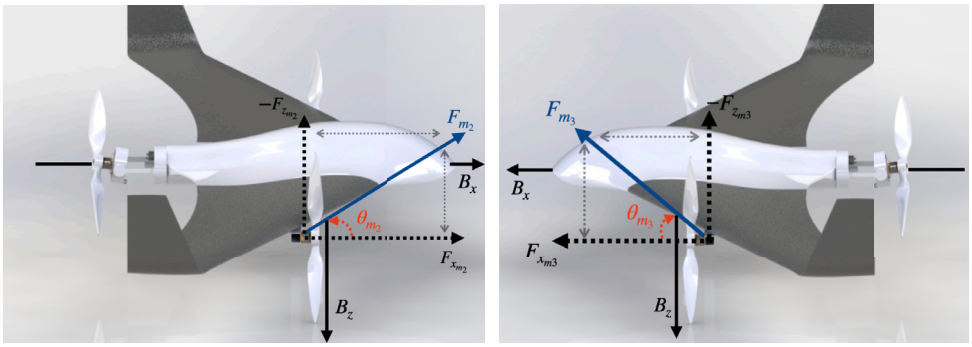

(a) Motor 2. (b) Motor 3.

Fig. 4. Thrust forces F_{m_2}, F_{m_3} in motors 2 and 3 and their decomposition in the B_x and B_z axes.

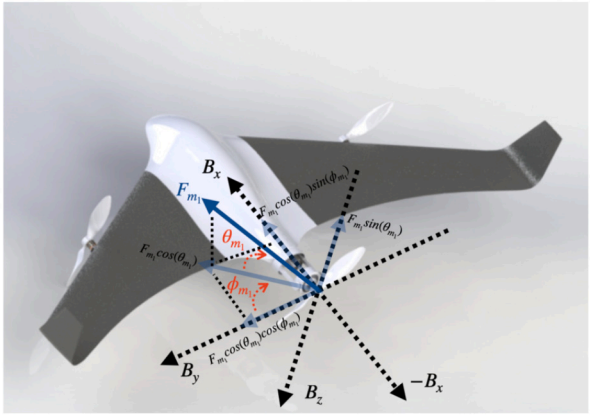

Fig. 5. Thrust forces F_{m_2}, F_{m_3} in motors 2 and 3 and their decomposition in the B_x and B_z axes.

$$F_x = K_F\Omega_1^2 \cos\theta_{m_1} \sin\psi_{m_1} + K_F\Omega_2^2 \cos\theta_{m_2} + K_F\Omega_3^2 \cos\theta_{m_3}; \tag{4}$$

$$F_y = -K_F\Omega_1^2 \cos\theta_{m_1} \cos\psi_{m_1}; \tag{5}$$

$$F_z = K_F\Omega_1^2 \sin\theta_{m_1} + K_F\Omega_2^2 \sin\theta_{m_2} + K_F\Omega_3^2 \sin\theta_{m_3}. \tag{6}$$

The forces generated by motor 1 are obtained by taking Fig. 5 as a reference. The main difference with respect to motors 2 and 3 is that motor 1 has a thrust vector at the rear, which adds one more degree of freedom. Therefore the forces generated are decomposed into more axes of motion, and the angles used to represent the inclination of the vectored thrust with two degrees of freedom were θ_{m_1} and ψ_{m_1}.

Thus, considering that motors 1 and 3 rotate clockwise and that motor 2 rotates counterclockwise, the components of the aerodynamic momentum are given by:

$$M_x = L_3(K_F\Omega_2^2 \sin\theta_{m_2} - K_F\Omega_3^2 \sin\theta_{m_3}); \tag{7}$$

$$M_y = L_2(K_F\Omega_2^2 \sin\theta_{m_2} + K_F\Omega_3^2 \sin\theta_{m_3}) - L_1K_F\Omega_1^2 \sin\theta_{m_1}; \tag{8}$$

$$M_z = L_3(K_F\Omega_2^2 \cos\theta_{m_2} - K_F\Omega_3^2 \cos\theta_{m_3}) - K_M\Omega_1^2 \sin\theta_{m_1} - K_M\Omega_3^2 \sin\theta_{m_3} + K_M\Omega_2^2 \sin\theta_{m_2} + K_F\Omega_1^2 \cos\theta_{m_1} \cos\psi_{m_1}; \tag{9}$$

where L_1, L_2 and L_3 represent the distance between the center of mass and the motors and these are obtained by measurement. K_F and K_M are the aerodynamic force and aerodynamic moment coefficients, respectively. Ω_1, Ω_2 and Ω_3 represent the angular velocity of motors 1, 2 and 3.

In the same way, the moments generated by the rotation of the motors represented in Eqs. (7)-(9) were modeled taking as reference the directions of rotation of each of the axes of motion, following the mechanical convention of the right hand, these directions can be seen in Fig. 6.

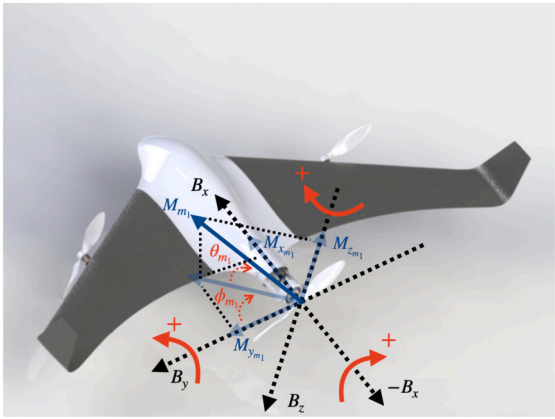

Fig. 6. Thrust moment M_{m_1} involved in motor 1 and its decomposition in the B_x, B_y and B_z axes.

3. Passivity-Based Control

Passivity Based Control is a well-known technique that exploits the physical restrictions of the system and, in particular, its energy dissipation properties.

The mathematical model represented in (3) is considered as a fully actuated system. Thus, we can develop a passivity-based control. The total energy of the system is defined as:

$$H(\lambda, \dot{\lambda}) = \frac{1}{2}\dot{\lambda}^T \Delta \dot{\lambda} + V(\lambda); \tag{10}$$

where Δ is the inertia matrix of the system and $V(\lambda)$ represents the potential energy:

$$V(\lambda) = mgz.$$

In the passivity-based control approach, the control input δ is decomposed into two terms: the first is the energy shaping (δ_{es}), and the second term represents the damping injection (δ_{di}), i.e.,

$$\delta = \delta_{es} + \delta_{di}. \tag{11}$$

A δ_{es} is required such that:

$$-\int_0^T \delta_{es}^T[\lambda(t)]y(t)dt = H_a[\lambda(t)] + k; \tag{12}$$

with $k > 0$ is the constant of integration. The desired Hamiltonian is:

$$H_d(\lambda, \dot{\lambda}) = H(\lambda, \dot{\lambda}) + H_a(\lambda); \tag{13}$$

where $H_a(\lambda)$ represents the energy supplied by the controller. Therefore, it is required that the function H_d has an isolated minimum called λ_*, i.e., $\lambda_* = \arg\min H_d(\lambda, \dot{\lambda})$.

The energy shaping term is expressed as follows [19,20]:

$$\delta_{es} = \nabla_\lambda H(\lambda, \dot{\lambda}) - K_p(\lambda - \lambda_*); \tag{14}$$

where $\nabla_\lambda H = \partial H / \partial \lambda$, is the gradient of the Hamiltonian with respect to the generalized coordinate, $K_p = K_p^T > 0$ is the gain matrix of energy shaping. Substituting (14) and the passive outputs $y = \dot{\lambda}$ into (12) and solving for $H_a(\lambda)$, we obtain:

$$H_a(\lambda) = -V(\lambda) + \frac{1}{2}(\lambda - \lambda_*)K_p(\lambda - \lambda *) + k. \tag{15}$$

Substituting (10) and (15) in (13) we obtain:

$$H_d(\lambda, \dot{\lambda}) = \frac{1}{2}\dot{\lambda}^T \Delta \dot{\lambda} + \frac{1}{2}(\lambda - \lambda_*)K_p(\lambda - \lambda_*). \tag{16}$$

Therefore, the energy shaping term can be rewritten as follows:

$$\delta_{es} = \nabla_\lambda H(\lambda, \dot{\lambda}) - \nabla_\lambda H_d(\lambda, \dot{\lambda}). \tag{17}$$

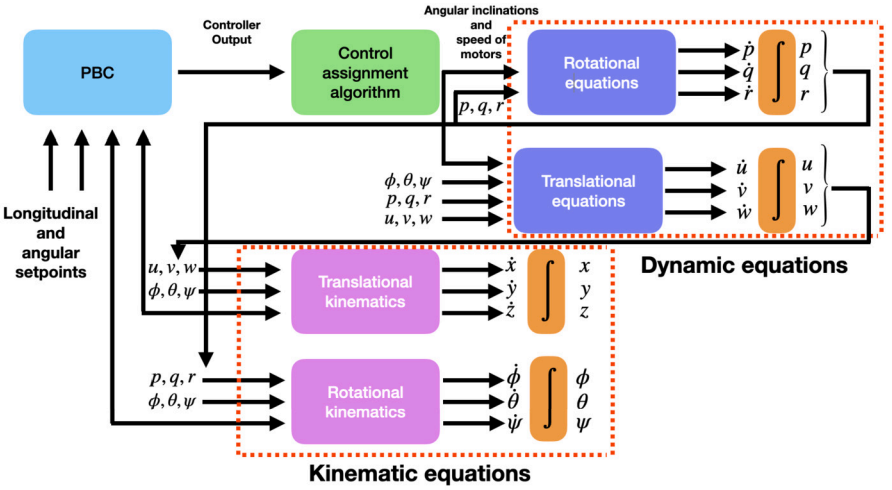

Fig. 7. Block diagram of the passivity-based controller where the control assignment algorithm allows decoupling of the angles of the front motors for independent functioning.

Now, we can determine δ_{es} for the convertible VTOL from (17):

$$\delta_{es}(\lambda) = m\bar{g} - K_p\left(\lambda - \lambda_*\right); \tag{18}$$

where $\bar{g} = \begin{bmatrix} 0 & 0 & 0 & g & 0 & 0 \end{bmatrix}^T$, $K_p = \begin{bmatrix} K_{p_1} & 0_{3\times3} \\ 0_{3\times3} & K_{p_2} \end{bmatrix}$, $K_{p_1} = diag\begin{bmatrix} 23 & 28 & 23 \end{bmatrix}$ and $K_{p_2} = diag\begin{bmatrix} 46 & 57 & 46 \end{bmatrix}$.

For the damping injection we have:

$$u_{di}(\dot{\delta}) = -K_v\left(\dot{\lambda} - \dot{\lambda}_*\right); \tag{19}$$

where $K_v = K_v^T = diag\begin{bmatrix} 10 & 15 & 10 & 18 & 22 & 18 \end{bmatrix}$.

The controller obtained from Eqs. (18) and (19) provide 6 virtual inputs, however, the convertible VTOL system has 7 real inputs, in order to transform these virtual inputs into real inputs, a control assignment algorithm is detailed in the following subsection.

3.1. Control assignment algorithm

The proposed control scheme for a convertible VTOL has a structure based on the PBC strategy, where the system is considered fully actuated. It generates the corresponding control signals for the translational and angular position of the vehicle considering the scheme presented in Fig. 7.

The control assignment algorithm allows the decoupling of the angles of the front motors so that they can be different from each other.

Considering the structure of aerodynamic forces and moments in translation and rotation dynamics, the input F_z is directly related to altitude control, the torque inputs M_y and M_x are used for pitch and roll control, which provide the set points for angular position control, while the input M_z is directly related to yaw motion control and finally, F_x and F_y control the desired longitudinal positions. Therefore, for a convertible VTOL system, let δ_m be the vector of manipulated inputs defined by

$$\delta_m = \begin{bmatrix} \Omega_1^2 & \Omega_2^2 & \Omega_3^2 & \theta_{m_1} & \psi_{m_1} & \theta_{m_2} & \theta_{m_3} \end{bmatrix}^T;$$

where Ω_{m_i} represents the angular velocities of each motor, θ_{m_i} the angular positions of each motor around the Y-axis with respect to B and ψ_{m_1} the rotation with respect to the Z-axis of the thrust vector.

Let u be an intermediate control input given by

$$u = \begin{bmatrix} \Omega_1^2 \sin\theta_{m_1} \\ \Omega_1^2 \cos\theta_{m_1} \cos\psi_{m_1} \\ \Omega_1^2 \cos\theta_{m_1} \sin\psi_{m_1} \\ \Omega_2^2 \sin\theta_{m_2} \\ \Omega_2^2 \cos\theta_{m_1} \\ \Omega_3^2 \sin\theta_{m_3} \\ \Omega_3^2 \cos\theta_{m_3} \end{bmatrix}.$$

The relationship between δ and u is provided by the mixing matrix Υ as follows:

$$\delta = \Upsilon u;$$

where

$$\Upsilon = \begin{bmatrix} 0 & 0 & K_F & 0 & K_F & 0 & K_F \\ 0 & -K_F & 0 & 0 & 0 & 0 & 0 \\ -K_F & 0 & 0 & -K_F & 0 & -K_F & 0 \\ 0 & 0 & 0 & L_3K_F & 0 & -L_3K_F & 0 \\ -L_1K_F & 0 & 0 & L_2K_F & 0 & L_2K_F & 0 \\ K_M & -L_1K_F & 0 & K_M & L_3K_F & K_M & -L_3K_F \end{bmatrix}.$$

Finally, the components of the manipulated control input δ_m are obtained through trigonometric operations of the force decompositions in which each of the motors and the thrust vector were modeled:

$$\theta_{m_i} = \arctan\left(\frac{\Omega_i^2 \sin\theta_{m_i}}{\Omega_i^2 \cos\theta_{m_i}}\right);$$

$$\psi_{m_1} = \arctan\left(\frac{\Omega_1^2 \cos\theta_{m_1} \sin\phi_{m_1}}{\Omega_1^2 \cos\theta_{m_1} \cos\phi_{m_1}}\right);$$

$$\Omega_i^2 = \sqrt{(\Omega_i^2 \cos\theta_{m_i})^2 + (\Omega_i^2 \sin\theta_{m_i})^2}.$$

4. Numerical simulation results

In order to validate the control performance, we analyze the behavior of numerical simulations of the convertible vehicle control algorithm and the flight transition trajectories. The simulations were carried out using the Euler integration method with a step size of 0.0001.

4.1. Numerical simulations

In this first test, the transition between flight modes is performed. Thus, a vertical ascent trajectory was required (this trajectory can only be performed by a conventional VTOL and not by a fixed-wing aircraft), followed by a displacement in the X-axis.

Thus, the desired trajectory is:

$$\lambda_* = \begin{cases} \begin{bmatrix} 0 & 0 & -5 \end{bmatrix}^T, & 0 < t < 5 \\ \begin{bmatrix} 45 & 0 & -5 \end{bmatrix}^T, & 5 \le t < 15 \\ \begin{bmatrix} 45 & 0 & 0 \end{bmatrix}^T, & t \ge 15 \end{cases}$$

Fig. 8a illustrates the vehicle's x, y, and z positions. We can see how the aircraft ascends 5 m without moving along any of the X and Y axes, in the graph this is reflected with a negative sign due to the directions of the reference frame, then travels 45 m on the X-axis, and finally, the vehicle descends. It can be seen how, when moving along the X-axis a slight rise in the Y-axis is generated due to the lift coefficients produced by the wings when reaching the desired position of 45 m, which is quickly compensated by the controller.

Fig. 8b depicts the attitude dynamics of the convertible VTOL system, where we observe that the rotation converged to the desired points with a null steady-state error. The profiles of the control inputs are presented in Figs. 8c-8d. Finally, a three-dimensional view of the path followed by the vehicle is depicted in Fig. 8e. In general, this simulation shows an adequate transition between flight modes: vertical take-off, horizontal flight, and landing.

A second test was carried out. In this case, the desired trajectory is:

$$\lambda_* = \begin{cases} \begin{bmatrix} 0 & 0 & -5 \end{bmatrix}^T, & 0 < t < 3 \\ \begin{bmatrix} 2t & \sin(2t) & -5 \end{bmatrix}^T, & 3 \le t < 15 \\ \begin{bmatrix} 2t & 0 & 0 \end{bmatrix}^T, & 15 \le t \le 20 \end{cases}$$

In Fig. 9a, we can observe the positions of the vehicle. We can see that the position for each axis was stabilized according to the desired reference. Fig. 9b illustrates the angular response that the system has with respect to the desired angles, in which they practically remain at 0 degrees. In Fig. 9c, we can appreciate the angular positions of the motors, allowing the aircraft to stay without any inclination since they move to generate the forces required by the controller. And finally, a three-dimensional view of the path followed by the aircraft is shown in Fig. 9d, where we observe a good performance in the tracking of a vertical ascent, horizontal displacement while tracking a sinusoidal reference, vertical descent, and transitions between flight modes.

Finally, a third test was carried out. The desired trajectory is:

$$\lambda_* = \begin{bmatrix} 5\cos(t) & 5\sin(t) & t \end{bmatrix}^T, \quad 0 < t \le 100$$

Figs. 10a-10c show the tracking of an upward spiral for the convertible VTOL. We can observe that the developed control algorithm was capable of achieving accurate trajectory tracking since the vehicle converged to the reference trajectory.

Table 2 provides the Integral Time Absolute Error (ITAE) performance index of the result of the three tests shown above.

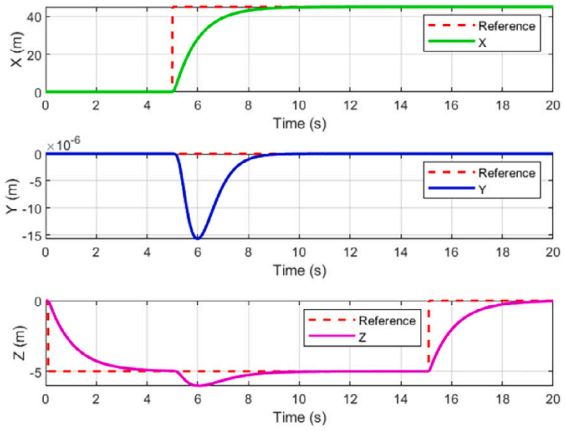

(a) Position.

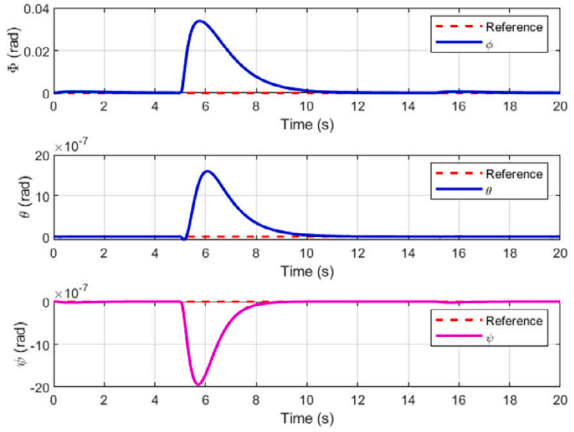

(b) Attitude.

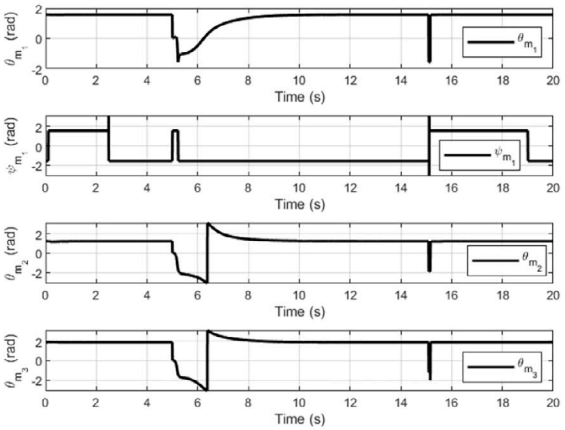

(c) Control inputs.

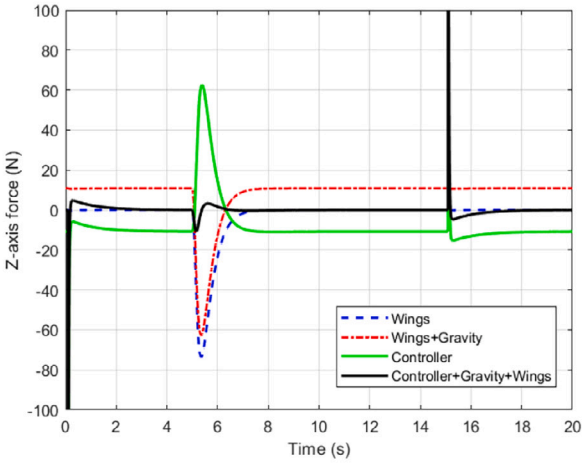

(d) Forces.

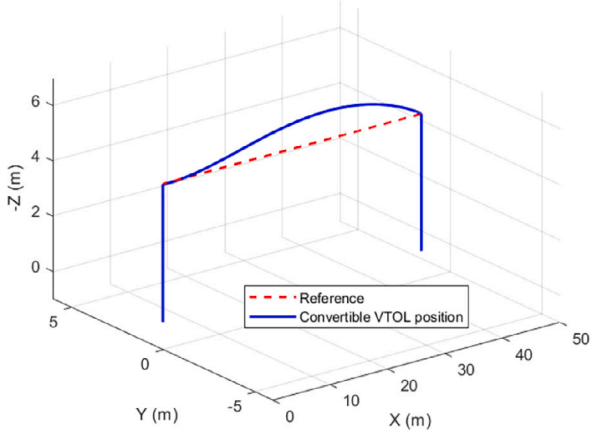

(e) Three-dimensional trajectory.

Fig. 8. Numerical results for the transition between flight modes: vertical take-off, horizontal flight, and landing.

In summary, the proposed controller has a relatively simple structure with a low computational burden. The numerical results show the good performance of the controller. Therefore, in the future, to carry out the validation of the proposed controller, we propose the use of a Skywalker X8 UAV equipped with onboard flight sensors that allow the measurement of the rotation angles and its velocities as well as a motion capture system that provides the spatial location of the vehicle.

Table 2
ITAE performance index.

Trajectory	x	y	z	ϕ	θ	ψ
Takeoff-translation-landing	830	0.001	20.5	0.002	0.03	0.0005
Sinusoidal	1230	20	8.75	12.3	0.56	0.0005
Upward spiral	1635	471.7	202.7	14.69	31.17	18.3

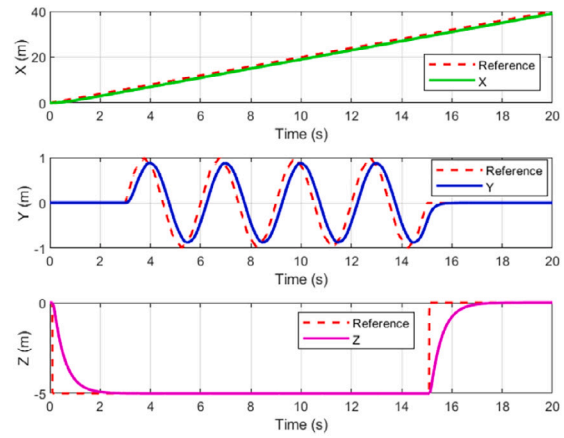

(a) Position.

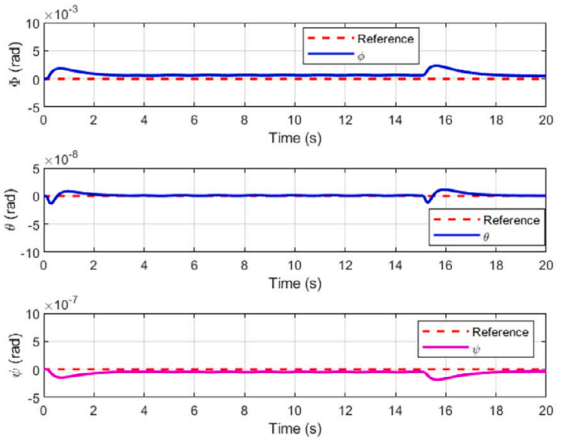

(b) Attitude.

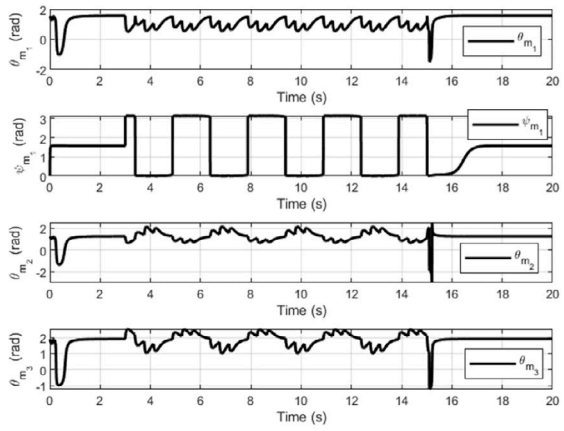

(c) Control inputs.

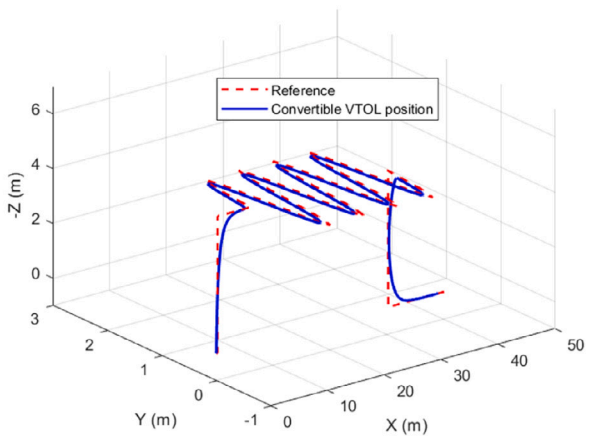

(d) Three-dimensional trajectory.

Fig. 9. Numerical results for the tracking of a vertical ascent, horizontal displacement while tracking a sinusoidal reference, vertical descent, and transitions between flight modes.

5. Conclusions

This work presented the development of a mathematical model and a passivity-based control strategy for a convertible UAV. The mathematical model was introduced in the Euler-Lagrange formulation, considering the aerodynamic parameters and the decomposition of forces generated by the designed thrust vector and the tilting motors. The PBC control algorithm presented good behavior in the translational and rotational position control, besides allowing the transition from cruise to stationary flight and vice-versa in the tested flight trajectories. A control assignment algorithm was then developed to relate the virtual control signals generated by the PBC to the real inputs of the system, which are the angular velocities of each motor and the tilt angles of the motors. The development of an experimental platform of the convertible fixed-wing UAV constitutes ongoing work where the aim is to validate the presented control algorithm through real-time experiments. Future work will look to improve the performance of the control algorithm in the presence of sensor noise, actuator faults, and wind disturbance. Also, it will focus on obstacle avoidance and trajectory tracking for the convertible fixed-wing VTOL as it has been described in [21,22] for other systems.

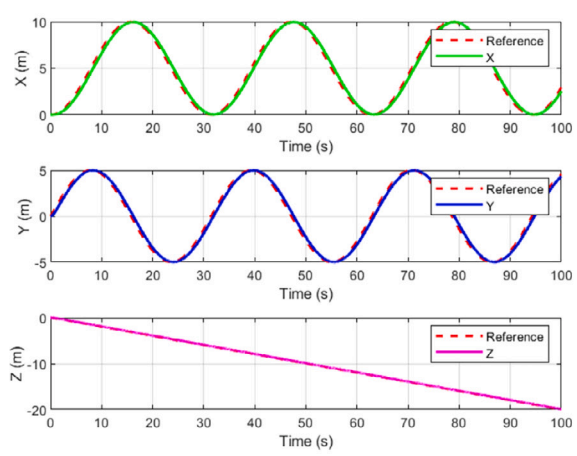

(a) Position.

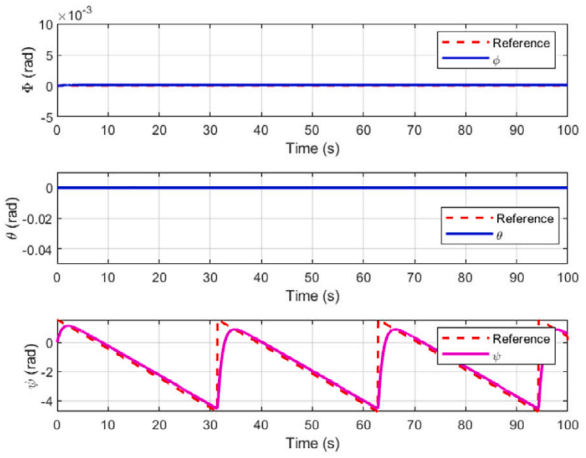

(b) Attitude.

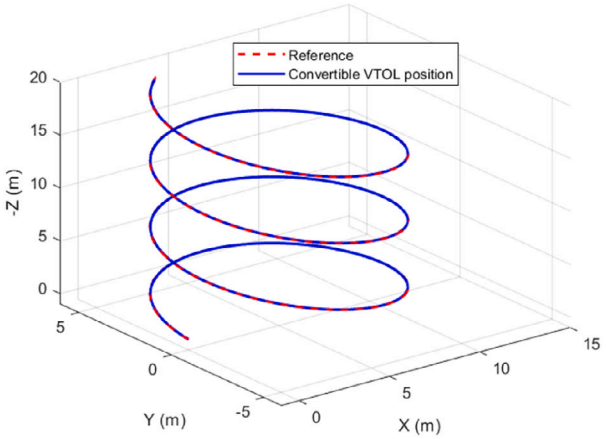

(c) Three-dimensional trajectory.

Fig. 10. Numerical results for tracking an upward spiral.

Funding

This work was supported by the Tecnológico Nacional de México under the program Proyectos de Investigación Científica, Desarrollo Tecnológico e Innovación. Additional support was provided by CONAHCYT through the program Investigadoras e Investigadores por México project 88 and the scholarship for the first author.

Data availability

No data was used for the research described in the article.

References

[1] K. Anderson, K.J. Gaston, Lightweight unmanned aerial vehicles will revolutionize spatial ecology, Front. Ecol. Environ. 11 (2013) 138–146, https://doi.org/10.1890/120150.

[2] P. Castillo, A. Dzul, R. Lozano, Real-time stabilization and tracking of a four-rotor mini rotorcraft, IEEE Trans. Control Syst. Technol. 12 (4) (2004) 510–516, https://doi.org/10.1109/TCST.2004.825052.

[3] N.Y. Ko, G. Song, W. Youn, S.H. You, Lie group approach to dynamic-model-aided navigation of multirotor unmanned aerial vehicles, IEEE Access 10 (2022) 72717–72730, https://doi.org/10.1109/ACCESS.2022.3180769.

[4] S. Fiori, L. Bigelli, F. Polenta, Lie-group type quadcopter control design by dynamics replacement and the virtual attractive-repulsive potentials theory, Mathematics 10 (7) (2022), https://www.mdpi.com/2227-7390/10/7/1104.

[5] C. Papachristos, K. Alexis, A. Tzes, Hybrid model predictive flight mode conversion control of unmanned quad-tiltrotors, in: 2013 European Control Conference (ECC), 2013, pp. 1793–1798.

[6] J.A. Bautista, A. Osorio, R. Lozano, Modeling and analysis of a tricopter/flying-wing convertible UAV with tilt-rotors, in: 2017 International Conference on Unmanned Aircraft Systems (ICUAS), 2017, pp. 672–681.

[7] Y. Wang, Y. Zhou, C. Lin, Modeling and control for the mode transition of a novel tilt-wing UAV, Aerosp. Sci. Technol. 91 (2019) 593–606, https://doi.org/10.1016/j.ast.2019.05.046.

[8] N.T. Hegde, V.I. George, C.G. Nayak, Modeling and transition flight control of vertical take-off and landing unmanned tri-tilting rotor aerial vehicle, in: 2019 3rd International Conference on Electronics, Communication and Aerospace Technology (ICECA), 2019, pp. 590–594.
[9] L.M. Sanchez-Rivera, R. Lozano, A. Arias-Montano, Transition flight dynamics of a dual tilt-wing UAV, in: 2020 International Conference on Unmanned Aircraft Systems (ICUAS), 2020, pp. 862–866.
[10] B. Li, J. Sun, W. Zhou, C.-Y. Wen, K.H. Low, C.-K. Chen, Transition optimization for a VTOL tail-sitter UAV, IEEE/ASME Trans. Mechatron. 25 (5) (2020) 2534–2545, https://doi.org/10.1109/TMECH.2020.2983255.
[11] L. Spannagl, G. Ducard, Control allocation for an unmanned hybrid aerial vehicle, in: 2020 28th Mediterranean Conference on Control and Automation (MED), 2020, pp. 709–714.
[12] L. Bauersfeld, L. Spannagl, G.J.J. Ducard, C.H. Onder, Mpc flight control for a tilt-rotor VTOL aircraft, IEEE Trans. Aerosp. Electron. Syst. 57 (4) (2021) 2395–2409, https://doi.org/10.1109/TAES.2021.3061819.
[13] J. Chi, Y. Wang, Q. Chen, P. Wang, Z. Hou, Controller design and flight test of the high-lift hybrid mode UAV, in: 2022 6th International Conference on Robotics and Automation Sciences (ICRAS), 2022, pp. 62–67.
[14] L. Bauersfeld, G. Ducard, Fused-PID control for tilt-rotor VTOL aircraft, in: 2020 28th Mediterranean Conference on Control and Automation (MED), 2020, pp. 703–708.
[15] M. Allenspach, G.J.J. Ducard, Nonlinear model predictive control and guidance for a propeller-tilting hybrid unmanned air vehicle, Automatica 132 (2021) 109790, https://doi.org/10.1016/j.automatica.2021.109790.
[16] K. Gryte, R. Hann, M. Alam, J. Roháč, T.A. Johansen, T.I. Fossen, Aerodynamic modeling of the Skywalker X8 fixed-wing unmanned aerial vehicle, in: 2018 International Conference on Unmanned Aircraft Systems (ICUAS), 2018, pp. 826–835.
[17] S.H. Mathisen, K. Gryte, T. Johansen, T.I. Fossen, Non-linear Model Predictive Control for Longitudinal and Lateral Guidance of a Small Fixed-Wing UAV in Precision Deep Stall Landing, Ch. Session: Unmanned Systems - Flight Dynamics and Control, American Institute of Aeronautics and Astronautics, 2016, pp. 1–16, https://arc.aiaa.org/doi/abs/10.2514/6.2016-0512.
[18] R. Beard, T. McLain, Small Unmanned Aircraft: Theory and Practice, Princeton University Press, 2012, https://arc.aiaa.org/doi/abs/10.2514/6.2016-0512.
[19] R. Ortega, I. Mareels, Energy-balancing passivity-based control, in: Proceedings of the 2000 American Control Conference, ACC (IEEE Cat. No.00CH36334), vol. 2, 2000, pp. 1265–1270.
[20] R. Ortega, A. Van Der Schaft, I. Mareels, B. Maschke, Putting energy back in control, IEEE Control Syst. Mag. 21 (2) (2001) 18–33, https://doi.org/10.1109/37.915398.
[21] A.H. Khan, S. Li, X. Luo, Obstacle avoidance and tracking control of redundant robotic manipulator: an RNN-based metaheuristic approach, IEEE Trans. Ind. Inform. 16 (7) (2020) 4670–4680, https://doi.org/10.1109/TII.2019.2941916.
[22] A.H. Khan, S. Li, D. Chen, L. Liao, Tracking control of redundant mobile manipulator: an RNN based metaheuristic approach, Neurocomputing 400 (2020) 272–284, https://doi.org/10.1016/j.neucom.2020.02.109.